Beyond Lambert: Reconstructing Surfaces with Arbitrary BRDFs*

Sebastian Magda
David J. Kriegman
Beckman Institute
Computer Science
University of Illinois, Urbana-Champaign
Urbana, IL 61801

Todd Zickler
Peter N. Belhumeur
Center for Comp. Vision & Control
EE and CS
Yale University
New Haven, CT 06520-8267

Abstract

We address an open and hitherto neglected problem in computer vision, how to reconstruct the geometry of objects with arbitrary and possibly anisotropic bidirectional reflectance distribution functions (BRDFs). Present reconstruction techniques, whether stereo vision, structure from motion, laser range finding, etc. make explicit or implicit assumptions about the BRDF. Here, we introduce two methods that were developed by re-examining the underlying image formation process; the methods make no assumptions about the object's shape, the presence or absence of shadowing, or the nature of the BRDF which may vary over the surface. The first method takes advantage of Helmholtz reciprocity, while the second method exploits the fact that the radiance along a ray of light is constant. In particular, the first method uses stereo pairs of images in which point light sources are co-located at the centers of projection of the stereo cameras. The second method is based on double covering a scene's incident light field; the depths of surface points are estimated using a large collection of images in which the viewpoint remains fixed and a point light source illuminates the object. Results from our implementations lend empirical support to both techniques.

1 Introduction

We address an open problem in computer vision: how to reconstruct the shape (geometry) of an object with an arbitrary, unknown bidirectional reflectance distribution function (BRDF) [8]. Our solutions stand in contrast to existing methods which assume, either implicitly or explicitly, that the BRDF of points on the object's surface are Lambertian, approximately Lambertian, or of some known parametric form.

A BRDF at a point on the surface is the ratio of the outgoing radiance to the incident irradiance. The BRDF can be represented as a positive 4-D function $\rho(\hat{\mathbf{i}}, \hat{\mathbf{e}})$ where $\hat{\mathbf{i}}$ is the direction of an incident light ray, and $\hat{\mathbf{e}}$ is the direction of the outgoing ray. The coordinates of $\hat{\mathbf{i}}$ and $\hat{\mathbf{e}}$ are usually expressed with respect to a coordinate system attached to the tangent plane. The BRDF is not an arbitrary function since from the second law of thermodynamics, it satisfies Helmholtz's reciprocity condition $\rho(\hat{\mathbf{i}}, \hat{\mathbf{e}}) = \rho(\hat{\mathbf{e}}, \hat{\mathbf{i}})$ [8]. This symmetry essentially says that the fraction of light coming from direction $\hat{\mathbf{i}}$ and emitted in direction $\hat{\mathbf{e}}$ is the same as that coming from $\hat{\mathbf{e}}$ and emitted in direction $\hat{\mathbf{i}}$.

*D. Kriegman and S. Magda were supported by NSF ITR CCR 00-86094 and DAAH04-95-1-0494. P. N. Belhumeur was supported by a Presidential Early Career Award IIS-9703134, NSF KDI-9980058, NIH R01-EY 12691-01, and an NSF ITR.

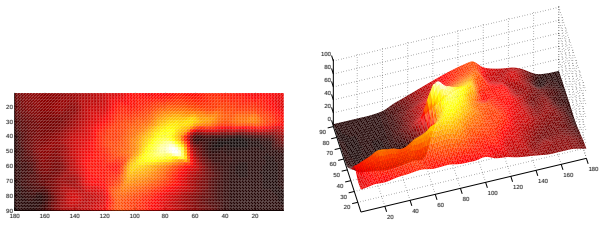

Figure 1: The measured intensity of one pixel as a function of light source position. Images were acquired as a point source was moved over a quarter of a sphere.

In computer vision and computer graphics, models are used to simplify the BRDF. In computer vision, Lamberts Law is the basis for most reconstruction techniques. And, in computer graphics it would not be an exaggeration to say that more than 99.99% of rendered images use a Phong reflectance model which is composed of an ambient term, a diffuse (Lambertian) term and an ad hoc specular term [18]. While the isotropic Phong model captures the reflectance properties of plastics over a wide range of conditions, it does not effectively capture the reflectance of materials such as metals and ceramics, particularly when they have rough (random) surfaces or a regular surface structure (e.g., parallel grooves). Much less common are a number of physics-based parametric models [12, 17, 21], yet each of these only characterizes a limited class of surfaces. So, a recent alternative is to measure the BRDF and represent it by a suitable set of basis functions [11].

As a simple empirical illustration of the complexity of the BRDF's of real surfaces, consider the two views of a surface plot shown in Fig. 1. For a ceramic figurine, this plot shows the measured intensity of one pixel as an isotropic point source is moved over a quarter of a sphere at approximately a constant distance from the surface. While the deep rectangular cutout (dark part) is attributable to self shadowing, note that the rest

of surface lacks the characteristic lobes in reflectance models such as Phong.

For a surface whose BRDF is not a function of $\hat{\mathbf{e}}$ (i.e., Lambertian), the image intensity of a surface point will be the same irrespective of the viewing direction. This "constant brightness assumption" is the basis for establishing correspondence in dense stereo and motion methods. Yet for objects with a general and unknown BRDFs, this constant brightness assumption is violated. Thus, establishing correspondences between images gathered from different viewpoints under constant lighting is difficult – if not impossible. Methods for computing optical flow (e.g., Horn and Schunck [8]) also assume constant brightness.

Similarly, nearly all photometric stereo methods assume that the BRDF is Lambertian [13, 19, 22], is completely known a priori, or can be specified using a small number of parameters usually derived from limited physical models [7, 9, 16, 20]. In these methods, multiple images under varying lighting (but fixed viewpoint) are used to estimate a field of surface normals which is then integrated to produce a surface. When the BRDF varies across the surfaces, there is insufficient information to reconstruct both the geometry and the BRDF. Naturally with only a single image, shape-from-shading methods are even more limited. In [14], a hybrid method with controlled lighting and object rotation was used to estimate both the structure and a non-parametric reflectance map, though the BRDF must be isotropic and uniform across the surface.

Even the effectiveness of structured light methods such as triangulation-based light stripers and laser range finders depends upon the BRDF. While it is no longer necessary to paint an object matte white to obtain effective range scans from light stripers, specularities and interreflections tend to cause erroneous depth readings for metallic objects. Similarly, when the surface is specular and there is little backscatter, there may be insufficient return for a laser range finder to estimate depth. There are numerous other reconstruction techniques, yet their effectiveness also depends upon explicit or implicit assumptions about the BRDF.

The only techniques that do not seem to impose any requirements on the BRDF are shape-from-silhouette (by deformation of the occluding contour) and shape-from-shadows methods. However, silhouette-based methods are limited to surface points on the visual hull, and implementations of shape-from-shadow algorithms are not yet particularly effective.

In contrast, we present two new methods for recovering the geometry of objects with an arbitrary BRDF. In both cases, we assume a local reflectance model and ignore the secondary effects of interreflection. The first technique uses a modest set of images of a scene acquired from multiple viewpoints with controlled illumination. The second technique uses a large number of images acquired from a single viewpoint, but under different lighting conditions. While more data intensive, this technique can yield a 2-D slice of the 4-D BRDF at each reconstructed surface point which can then be used for photorealistic image-based rendering [15].

The first method requires as few as two images of the object/scene taken from differing viewpoints under differing lighting conditions. The method is essentially a form of binocular (or multinocular) stereopsis in which the lighting is controlled in such a manner as to exploit Helmholtz reciprocity. If only two images are used, image acquisition proceeds in two simple steps. First, an image is acquired with the object/scene illuminated by a single point light source. Second, the positions of the camera and light source are swapped, and the second image is acquired. After swapping, the point light source occupies the former position of the camera's focal point, while the focal point occupies the former position of the point light source. By acquiring the images in this manner, we ensure (up to contributions from interreflections) that for all corresponding points in the images, the ratio of the outgoing radiance to the incident irradiance is the same. Note that in general this is **not true** for stereo pairs – unless the surfaces of the objects have Lambertian reflectance.

The second method requires only a single viewpoint of the object, but *many* images of the object illuminated by point light sources at different positions. In particular, we require two sets of images of the object: an inner and an outer set. The inner set of images is created by moving a point light source over any known surface that is star-shaped (e.g., convex) with respect to all object points. The outer set of images is similarly acquired with light sources on a second non-intersecting star-shaped surface. Using these two sets of images, a point for point reconstruction of the object's visible surface is performed by estimating the depth of each point along the line of sight. Depth estimation is based on a simple assumption: the radiance along a ray of light is constant. With this assumption in hand, we reconstruct the surface by double covering the incident light field at the visible surface (the space of light rays). In particular, we are able to equate the scene radiance of an object point produced by a point light source lying on the inner star-shaped surface with the point's scene radiance produced by some corresponding point light source lying on the outer star-shaped surface. The correct correspondence can then be cast as a 1-D optimization over the point's depth along the line of sight.

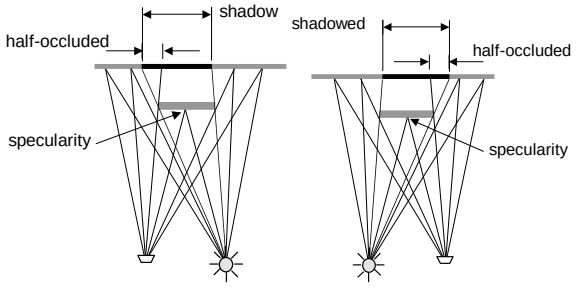

a. b.

Figure 2: The setup for acquiring a pair of images that exploits Helmholtz reciprocity: a. An image is acquired with the scene illuminated by a single point light source. b. Second image is acquired after the positions of the camera and light source are swapped.

2 Reciprocity Stereopsis

In this section we present a method for reconstructing surfaces with arbitrary BRDF's (e.g., non-Lambertian) using binocular (or multinocular) stereopsis. The method differs from standard stereopsis in that the illumination of the scene is chosen to exploit Helmholtz reciprocity [8]. Images are gathered by interchanging the positions of the light source and the camera's focal point as shown in Fig. 2.

The method offers two advantages over standard stereo arrangements. First, the image intensities of corresponding points in the images do not depend on the direction from which they are viewed – specularities and other non-Lambertian radiometric events appear fixed to the surface of the object as seen in the images. Thus, specularities may become powerful features which can actually aid in solving the stereo matching problem. This is in direct contrast with conventional stereo matching in which the illumination is fixed. In the latter case, specularities are located at different points on the object [4]. The second advantage of our method is that the shadowed and half-occluded regions are in correspondence – if a point is in shadow in the left image, it is not visible in the right image, and vice versa. Thus, if one uses a stereo matching algorithm that exploits the presence of half-occluded regions for determining depth discontinuities [1, 3, 5, 6], then these shadowed regions may significantly enhance the quality of the depth reconstruction. These stereo matching algorithms are designed to resolve the unmatchable half-occluded regions by introducing depth (or disparity) discontinuities at the shadow's edge.

Let us consider a calibrated multinocular stereo system composed of n pinhole cameras whose centers of projection are located at $\mathbf{o}_c$ for $c = 1 \cdots n$. From a calibration procedure, the multi-view epipolar geometry can be established. As in trinocular stereo, given a point $\mathbf{q}_1$ in image one, there is a one-parameter family of (n-1)-point sets $\{\mathbf{q}_2, ..., \mathbf{q}_n\}$ in the other images that could correspond to $\mathbf{q}_1$. Like disparity in binocular stereopsis, let d parameterize this family; in images $m = 2 \cdots n$, the $n-1$ points lying on the epipolar lines corresponding to $\mathbf{q}_1$ are given by $\mathbf{q}_m(d)$. To find correspondences, this family is searched, typically by choosing discrete values for d. For a Lambertian surface, the image intensity at $\mathbf{q}_1$ (or a small window around $\mathbf{q}_1$) is compared to the image intensities at $\mathbf{q}_m(d)$ for $m = 2 \cdots n$. Alternatively, some stereo methods match filtered intensities (e.g., normalized cross-correlation) or a vector of filtered intensities [10]. For a calibrated system, the 3-D location of the surface point $\mathbf{p}(d)$ can be determined for each value of d. We now develop an alternative matching constraint – one that that can be used for any BRDF.

Consider n isotropic point light sources to be colocated at the camera centers – this can be accomplished using mirrors or approximated by placing each light source near a camera. Images are acquired in the following fashion. Light source l is turned on while the other sources are turned off, and $n-1$ images are acquired from all cameras but camera l. This process is repeated n times until $n(n-1)$ images are acquired. Figure 2 shows this situation for a binocular system.

We now consider a constraint (a necessary condition) that can be used to determine if the image points $\mathbf{q}_m(d)$ from n cameras correspond to the same scene point $\mathbf{p}$ for some value of d. Let $\hat{\mathbf{v}}_c = \frac{1}{|\mathbf{o}_c - \mathbf{p}|}(\mathbf{o}_c - \mathbf{p})$ denote the direction from $\mathbf{p}$ to camera (or light source) c. The image irradiance in camera c when $\mathbf{p}$ is illuminated by light source l is given by

$$i_{c,l} = \eta \rho(\hat{\mathbf{v}}_l, \hat{\mathbf{v}}_c) \hat{\mathbf{n}} \cdot \hat{\mathbf{v}}_l \frac{1}{|\mathbf{o}_l - \mathbf{p}|^2} \tag{1}$$

where $\hat{\mathbf{n}} \cdot \hat{\mathbf{v}}_l$ gives the cosine of the angle between the direction to the light source and the surface normal at $\mathbf{p}$, $\frac{1}{|\mathbf{o}_l - \mathbf{p}|^2}$ is the $1/r^2$ falloff from an isotropic point light source, ρ is the BRDF, and η is a proportionality constant between measured irradiance and scene radiance for radiometrically calibrated lenses.

Now, consider the reciprocal case where light source c at $\mathbf{o}_c$ is turned on, and camera l at $\mathbf{o}_l$ observes $\mathbf{p}$. In this case, the image irradiance is

$$i_{l,c} = \eta \rho(\hat{\mathbf{v}}_c, \hat{\mathbf{v}}_l) \hat{\mathbf{n}} \cdot \hat{\mathbf{v}}_c \frac{1}{|\mathbf{o}_c - \mathbf{p}|^2}. \tag{2}$$

Because of Helmholtz reciprocity, we have that $\rho(\hat{\mathbf{v}}_c, \hat{\mathbf{v}}_l) = \rho(\hat{\mathbf{v}}_l, \hat{\mathbf{v}}_c)$, and so we can eliminate the BRDF term in the above two equations to obtain

$$(i_{l,c}\mathbf{w}_l - i_{c,l}\mathbf{w}_c) \cdot \hat{\mathbf{n}} = 0 \tag{3}$$

where $\mathbf{w}_l = \frac{1}{|\mathbf{o}_l - \mathbf{p}|^2}\hat{\mathbf{v}}_l$ and $\mathbf{w}_c = \frac{1}{|\mathbf{o}_c - \mathbf{p}|^2}\hat{\mathbf{v}}_c$.

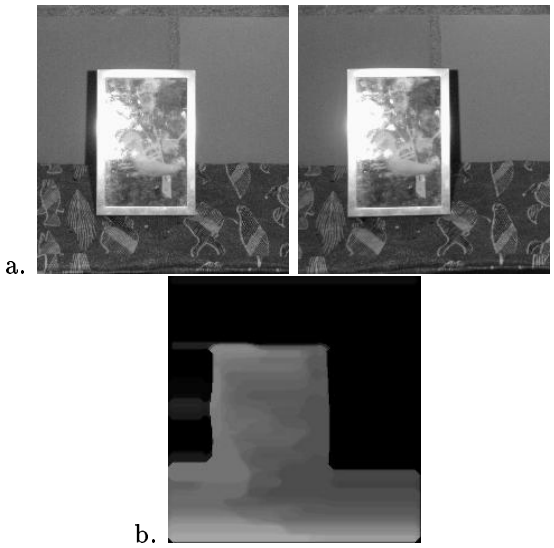

Figure 3: Result of Helmholtz reciprocity-based stereo: a. A stereo pair of images acquired by swapping the camera and light source. b. Disparity map.

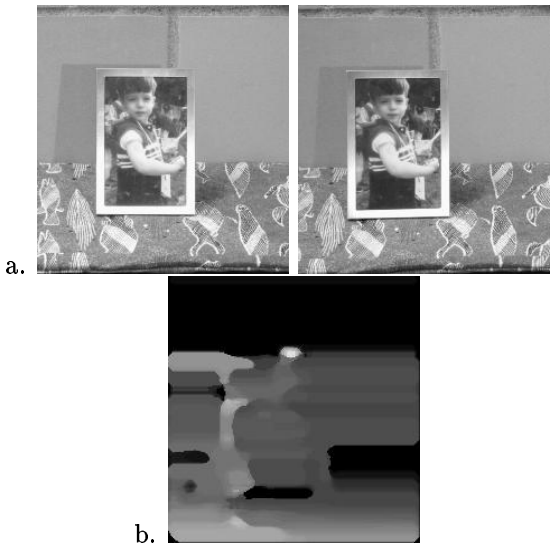

Figure 4: Result of conventional stereo: a. A stereo pair from the same camera positions as in Fig. 3, but under the fixed lighting. b. Disparity map.

In Eq. 3, $i_{l,c}$ and $i_{c,l}$ are measurements. For calibrated cameras and a value for the multinocular disparity d, $\mathbf{w}_c$ and $\mathbf{w}_l$ can be computed. So, only the surface normal $\hat{\mathbf{n}}$ is unknown.

For $n \geq 3$, we can form $n(n-1)/2$ linear constraints of this form. Let W be the $n(n-1)/2$ by 3 matrix whose rows are $(i_{l,c}\mathbf{w}_l - i_{c,l}\mathbf{w}_c)^T$, then these constraints can be expressed as

$$W\hat{\mathbf{n}} = 0. \tag{4}$$

Clearly, the surface normal lies in the null space of W, and it can be estimated from a noisy matrix using singular value decomposition. Alternatively, W should be rank 2, and this can be used as a necessary condition for establishing correspondence when searching the disparity d. Note that at least three camera/light source positions are needed to exploit this constraint.

2.1 Implementation and Results

To evaluate the use of Helmholtz reciprocity and colocating cameras and light sources, we have implemented a simplified version of this approach using a binocular pair of cameras observing a scene whose geometry is shown in Fig. 2. Since the constraint derived above requires at least a trinocular rig, we have chosen a camera and scene configuration in which we can make the following two approximations.

When the stereo rig has a small baseline with respect to the scene depth,

$$|\mathbf{o}_c - \mathbf{p}|^2 \approx |\mathbf{o}_l - \mathbf{p}|^2. \tag{5}$$

Also, if the surfaces are nearly fronto-parallel, we have

$$\hat{\mathbf{n}} \cdot \hat{\mathbf{v}}_l \approx \hat{\mathbf{n}} \cdot \hat{\mathbf{v}}_c \approx 1. \tag{6}$$

Using these approximation along with Helmholtz reciprocity, the BRDF can be eliminated from Eqs. 1 and 2 to obtain the matching constraint

$$i_{c,l} = i_{l,c}. \tag{7}$$

That is, correspondence can be established simply by comparing pixel intensities across the epipolar lines in the two images just as in standard stereo vision algorithms. Recall that unlike standard stereo, we have lit the scene differently for the two images.

Figure 3.a shows a stereo pair similar to the one illustrated in Fig. 2. Note that the specularities occur at the same locations in both images, as is predicted by Helmholtz reciprocity. Thus, the specularities become features in both images which can actually aid in establishing correspondence. Note again that the shadowed regions occur in the half-occluded regions in both images – if a point is in shadow in the left image, it is not visible in the right image, and vice versa.

To establish correspondence between the two images shown in Fig. 3.a, we have implemented the "World II" stereo algorithm described in [1]. We chose this algorithm both because it is intensity-based (not edge-based) and because it implicitly resolves half-occluded regions by linking them to depth (disparity) discontinuities. The result for our implementation of [1] applied to the stereo pair in Fig. 3.a is shown in Fig. 3.b.

We then gathered a new stereo pair as seen in Fig. 4.a in which the lighting was the same for both the left and right images. The stereo pair in Fig. 4.a differs from that in Fig. 3a only in the illumination – the positions of the cameras and scene geometry were identical.

The result for our implementation of [1] applied to the stereo pair in Fig. 4.a is shown in Fig. 4.b. Note that we used the same implementation of [1] to establish correspondences for the new pair of images. Although the accuracy of the stereo matching may have been improved by pre-filtering the images, we avoided this to make the point that image intensity is very much viewpoint dependent.

There are two things to note about the results. First, the Helmholtz images in Fig. 3 have significant specularities, yet they remain fixed in the images and do not hinder stereo matching. Contrast this with the images in Fig. 4. These also have specularities (as seen on the frame and on the glass) and non-Lambertian effects (as seen in the intensity change of the background wall), yet they move between images and significantly hinder matching. Second, there is little texture on the background wall, yet the Helmholtz images have shadows in the half-occluded regions which allow the stereo algorithm to estimate the depth discontinuity at the boundary of the picture frame.

3 Reconstruction from Light Fields

In this section, we present a surface reconstruction method that resembles photometric stereo in that a single viewpoint and multiple lighting directions are used. Yet, this method differs significantly in that depth, rather than surface normal, is directly estimated, and no assumptions are made about the BRDF.

Let us first consider a fixed calibrated pinhole camera observing a static scene; see Fig. 5. Let the coordinates of a point on the image plane be given by $\mathbf{q} \in \mathbb{R}^2$. For every $\mathbf{q}$, there is a line passing through the optical center $\mathbf{o}$ in the direction $\hat{\mathbf{r}}(\mathbf{q})$ which we call the line of sight of pixel $\mathbf{q}$. We obtain the function $\hat{\mathbf{r}}(\mathbf{q})$ during camera calibration, and $\mathbf{o}$ is taken as the origin. The image point $\mathbf{q}$ is the projection of a scene point $\mathbf{p}$ lying on the line defined by $\mathbf{o}$ and $\hat{\mathbf{r}}(\mathbf{q})$. The depth $\lambda(\mathbf{q})$ of $\mathbf{p}$ from $\mathbf{o}$ is unknown, and the relation can be expressed as

$$\mathbf{p}(\mathbf{q}, \lambda) = \lambda(\mathbf{q})\hat{\mathbf{r}}(\mathbf{q}) + \mathbf{o}. \tag{8}$$

The process of reconstruction is the estimation of the depth map $\lambda(\mathbf{q})$, in this case from images gathered under different lighting conditions. Since we will be able to independently estimate λ for each $\mathbf{q}$, we will drop $\mathbf{q}$ from our notation and write $\mathbf{p}$ as a function of the unknown depth λ.

Consider the scene to be illuminated by an isotropic point light source (not at infinity) whose location $\mathbf{s} \in \mathbb{R}^3$ is known. The direction of the light ray from $\mathbf{s}$ to $\mathbf{p}$ is $\hat{\mathbf{d}}(\mathbf{s}, \lambda) = \frac{1}{|\mathbf{p}(\lambda) - \mathbf{s}|}(\mathbf{p}(\lambda) - \mathbf{s})$, and the distance between $\mathbf{s}$ and $\mathbf{p}$ is $d(\mathbf{s}, \lambda) = |\mathbf{p}(\lambda) - \mathbf{s}|$. While the BRDF

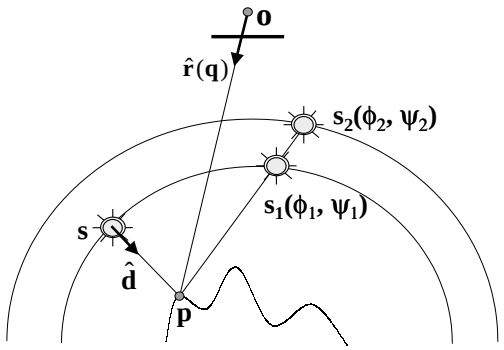

Figure 5: A 2-D schematic of the reconstruction setup. A camera whose origin is at $\mathbf{o}$ observes a scene point $\mathbf{p}$ which is illuminated by light sources covering two surfaces, parameterized as $\mathbf{s}_1(\phi_1, \psi_1)$ and $\mathbf{s}_2(\phi_2, \psi_2)$.

is typically defined with respect to a coordinate system attached to the surface's tangent plane, we will specify it in a global coordinate system as a function of the incoming light ray $\hat{\mathbf{d}}$ and the outgoing direction $-\hat{\mathbf{r}}$; i.e., we write the apparent BRDF as $\rho_a(\hat{\mathbf{d}}, \hat{\mathbf{r}})$. (Note that this apparent BRDF will include global properties of the scene like cast shadows.) While the relation between the incoming irradiance to the outgoing radiance is proportional to the true BRDF and the cosine between the incoming light and surface normal, we "fold" the cosine term into the apparent BRDF $\rho_a(\hat{\mathbf{d}}, \hat{\mathbf{r}})$.

The image intensity measured at $\mathbf{q}$ is a function of the light source intensity, $d^2(\mathbf{s}, \lambda)$ and $\rho_a(\hat{\mathbf{d}}, \hat{\mathbf{r}})$. Without loss of generality, we assume that all images are acquired with a unit intensity light source. The measured image intensity (irradiance) for image point $\mathbf{q}$ corresponding to a surface point at depth λ illuminated by light source $\mathbf{s}$ can be expressed as:

$$i(\mathbf{s}) = \frac{1}{d^2(\mathbf{s}, \lambda)} \rho_a(\hat{\mathbf{d}}(\mathbf{s}, \lambda), \hat{\mathbf{r}}). \tag{9}$$

As shown in Fig. 5, consider moving the light source over any known surface that is star-shaped with respect to all points on the object – any convex surface is sufficient. Parameterizing the surface by (ϕ_1, ψ_1), it can be expressed as $\mathbf{s}_1(\phi_1, \psi_1)$. For every light source position $\mathbf{s}_1(\phi_1, \psi_1)$, an image $I_1(\phi_1, \psi_1)$ is measured. Since we can treat each image location independently, we will simply denote the intensity measured at a single pixel by $i_1(\phi_1, \psi_1)$. Note that i_1 is a function of the light source position; Figure 1.a shows a surface plot for the intensity measured at one pixel as a light source is moved over a quarter sphere.

If the depth λ were known, then from the image data, a two-dimensional slice for fixed $\hat{\mathbf{r}}$ of the apparent BRDF at $\mathbf{p}$ could be determined from $\rho_a(\hat{\mathbf{d}}(\mathbf{s}, \lambda), \hat{\mathbf{r}}) = d^2(\mathbf{s}_1(\phi_1, \psi_1), \lambda) i_1(\phi_1, \psi_1)$. Alternatively, if the appar-

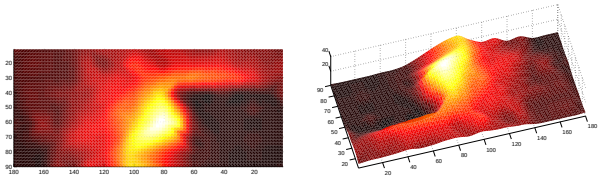

Figure 6: The measured intensity $i_2(\phi_2, \psi_2)$ of one pixel as a point light source is moved over the outer sphere. Compare to $i_1(\phi_1, \psi_1)$ in Fig 1 in which the light was moved over the inner sphere.

ent BRDF were known, then one could solve for the depth λ given the measured intensities $i_1(\phi_1, \psi_1)$ and the known light source positions $\mathbf{s}_1(\phi_1, \psi_1)$.

We now consider a method for simultaneously estimating the apparent BRDF and the depth. Let a second light source be moved on a second star-shaped surface which does not intersect the first one. Express this surface parametrically as $\mathbf{s}_2(\phi_2, \psi_2)$ and the corresponding measured images intensities as $i_2(\phi_2, \psi_2)$. Figure 6 shows a surface plot of the normalized intensity of the same pixel considered in Fig. 1 as the light source is moved over a second, outer sphere. Note that both surface plots reveal the same essential qualitative structure – the lower right corner is darkened, and the same ridge shape seems to be present. We will exploit this observation to reconstruct the depth.

For every light source position from the first (inner) surface $\mathbf{s}_1(\phi_1, \psi_1)$, there is a light source on the second (outer) surface $\mathbf{s}_2(\phi_2, \psi_2)$ where the ray from $\mathbf{p}$ through $\mathbf{s}_1(\phi_1, \psi_1)$ is collinear with the ray from $\mathbf{p}$ through $\mathbf{s}_2(\phi_2, \psi_2)$; see Fig. 5. We can express this correspondence of light sources on the two surfaces as a change of coordinates $\phi_2(\phi_1, \psi_1; \lambda)$ and $\psi_2(\phi_1, \psi_1; \lambda)$. This change of coordinates depends on the unknown location of $\mathbf{p}$, and so it is parameterized by the depth λ. That is, given the coordinates of a light source located on one surface and a depth λ, the location of the corresponding point on the second surface can be determined by this change of coordinates.

For such a pair of light sources $\mathbf{s}_1(\phi_1, \psi_1)$ and $\mathbf{s}_2(\phi_2, \psi_2)$, the value of the apparent BRDF $\rho_a(\hat{\mathbf{d}}, \hat{\mathbf{r}})$ is the same, and so the image intensities measured at pixel $\mathbf{q}$ are simply related by the relative $1/r^2$ loss from the isotropic point light source.

$$\begin{aligned} i_2(\phi_2, \psi_2) &= \frac{[d_1(\mathbf{s}_1(\phi_1, \psi_1), \lambda)]^2}{[d_2(\mathbf{s}_2(\phi_2, \psi_2), \lambda)]^2} i_1(\phi_1, \psi_1) \\ &= i_2(\phi_2(\phi_1, \psi_1; \lambda), \psi_2(\phi_1, \psi_1; \lambda)) \end{aligned} \quad (10)$$

This constraint between the intensities for corresponding light sources can be used to estimate the depth. The basic idea is that for a set of light sources located on one surface, we estimate the depth (and

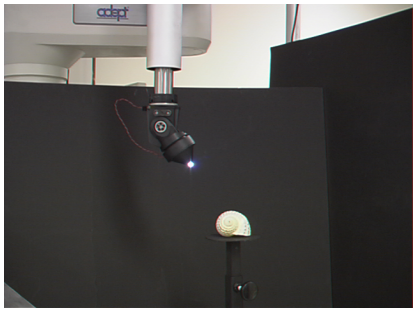

a.

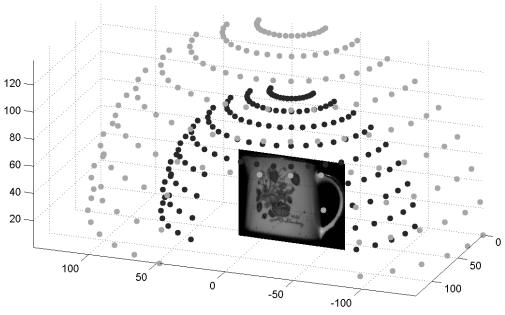

b.

Figure 7: Image acquisition: a. While a robot arm moves the point light source, images are acquired. b. Sample points cover a quarter of the inner and outer sphere of light source positions. The two cutouts correspond to positions where the arm occludes the camera.

therefore the change of coordinates and corresponding light source locations on the second surface) such that the respective image intensities satisfy the above constraint. This can be expressed as an objective function in the depth λ

$$\begin{aligned} \mathcal{O}(\lambda) = \int\int [& d_2^2(\lambda) i_2(\phi_2(\phi_1, \psi_1; \lambda), \psi_2(\phi_1, \psi_1; \lambda)) \\ & - d_1^2(\lambda) i_1(\phi_1, \psi_1)]^2 d\phi_1 d\psi_1. \end{aligned} \quad (11)$$

The depth λ is then found by minimizing $\mathcal{O}(\lambda)$, which would be zero at the true depth without image noise.

3.1 Implementation and Results

We have empirically validated this method using both a monochrome CCD camera and a white digital CCD camera. A 3-color LED source is accurately positioned using an ADEPT robot arm. See Figure 7.a.

The development of Eq. 11 is based on measuring the image intensity as a continuous function of the light source location. In practice, we obtain images by sampling the two surfaces of point light sources; in our experiments, the two surfaces were taken to be spheres enclosing the object. As shown in Fig. 7.b, a quarter of the sphere was sampled every ten degrees in latitude and longitude. However, a complication arises due to sampling. For most sampled light sources $\mathbf{s}_1(\phi_1, \psi_1)$ on the inner sphere, there is no corresponding sampled light source on the outer sphere

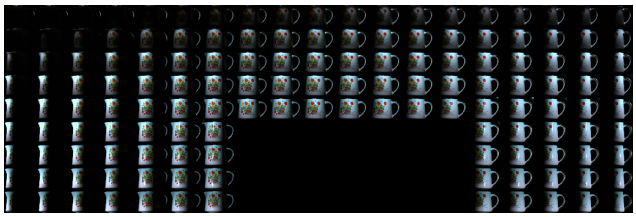

Figure 8: An example of 143 images with lights located on the inner sphere and used for reconstruction.

at $\mathbf{s}_2(\phi_2(\phi_1,\psi_1;\lambda),\psi_2(\phi_1,\psi_1;\lambda))$. So instead, we must interpolate from the available samples, and this is done as follows. The second surface is triangulated with the sample light source positions serving as vertices. Given $\mathbf{s}_1(\phi_1,\psi_1)$ and an estimated depth λ, we find the intersection $\mathbf{s}_2'(\phi_1,\psi_1)$ of the ray defined by $\mathbf{p}(\lambda)$ and $\mathbf{s}_1(\phi_1,\psi_1)$ with one of the triangles in the triangulation of the second surface. From the intensity values corresponding to the vertices and the coordinates of the light source of the vertices, bilinear interpolation is used to approximate the intensity $i_2'(\mathbf{s}_2')$.

The integral in Eq. 11 becomes a summation over n sampled light sources whose locations are $\mathbf{s}(\phi_1^j,\psi_1^j)$ on the first surface with corresponding pixel intensities $i_1(\phi_1^j,\psi_1^j)$. This gives the following objective function

$$\mathcal{O}'(\lambda) = \sum_{j=1}^{n}[d_2^2(\lambda)i_2'(\phi_2(\phi_1^j,\psi_1^j;\lambda),\psi_2(\phi_1^j,\psi_1^j;\lambda)) - d_1^2(\lambda)i_1(\phi_1^j,\psi_1^j)]^2. \quad (12)$$

There is no reason to expect Eq. 12 to be convex, but fortunately it is only a function of one variable λ, and it is bounded by the inner light source surface. Since $\mathcal{O}'(\lambda)$ is independent for each pixel, the depth of each pixel $\lambda(\mathbf{q})$ can be estimated independently.

Figure 8 shows a mosaic of 143 images of a ceramic pitcher illuminated by the light sources on the inner sphere positioned as shown in Fig. 7.b. The reconstruction method was applied to this object, and a depth map is shown in Fig. 9.a; note the small spout. Examples of a few other reconstructions of decidedly non-Lambertian objects can also be found in Fig. 9.

4 Discussion

This paper explores the issue of reconstructing the geometry of objects having an arbitrary (non-parametric) BRDF which may vary over the surface. By considering two well-known physical principles, Helmholtz reciprocity and the fact that radiance along a ray of light is constant, we have introduced two distinct methods for reconstructing the surface. Our main purpose was to show both algorithmically and empirically how these principles could be exploited for surface reconstruction. While both methods can reconstruct the surface geometry, the second method can also provide a 2-D slice of the 4-D BRDF, and this can be used for image-based rendering of the object under novel lighting conditions [2, 15]. The implemented algorithms are a first step in demonstrating the utility of these principles for surface reconstruction; there are a multitude of future directions to explore.

For the reciprocity-based stereo method, we have yet to fully implement the multinocular method without the approximations in Sec. 2.1. While we have considered a fully calibrated multinocular rig, is a full Euclidean reconstruction (rather than projective) possible for a geometrically uncalibrated camera system? Since the $1/r^2$ term in Eq. 1 provides a non-linear constraint on the camera center, a Euclidean reconstruction may still be possible. When acquiring images, we did not use images where the light source and camera center were co-located (i.e., $I_{c,l}$ with $c = l$). This "collinear light source" configuration was used in [14] and corresponds to a camera/source configuration lying on the symmetry set of the BRDF – i.e., self-reciprocal configurations.

For the light field-based reconstruction, there are also many avenues to explore. What is the relation of the BRDF and the geometry to the necessary sampling rate of light source positions? What are effective ways to render images and to extrapolate from a 2-D slice of the BRDF to the full BRDF? What can be gained from additional coverings of the incident light field? In our experiments, we used 8-bit cameras, yet the range of scene radiances is rather large in the presence of specularities; how would high dynamic range cameras/imaging help? Currently, this method requires that the light source positions be known. It would be preferable to simply "wave" a light over the object, and then to simultaneously estimate the light source positions and scene structure.

Finally, one wonders how the multi-view reciprocity-based method and the incident light field-based method can be merged to reconstruct both the surface geometry and the full 4-D BRDF.

References

[1] P. Belhumeur. A binocular stereo algorithm for reconstructing sloping, creased, and broken surfaces in the presence of half-occlusion. In *Int. Conf. on Computer Vision*, Berlin, Germany, 1993.

[2] P. Belhumeur and D. Kriegman. Shedding light on reconstruction and image-based rendering. Technical Report CSS-9903, Yale University, Center for Systems Science, New Haven, CT, Nov. 1999.

[3] P. Belhumeur and D. Mumford. A Bayesian treatment of the stereo correspondence problem using half-occluded regions. In *Proc. IEEE Conf. on Comp. Vision and Patt. Recog.*, pages 506–512, 1992.

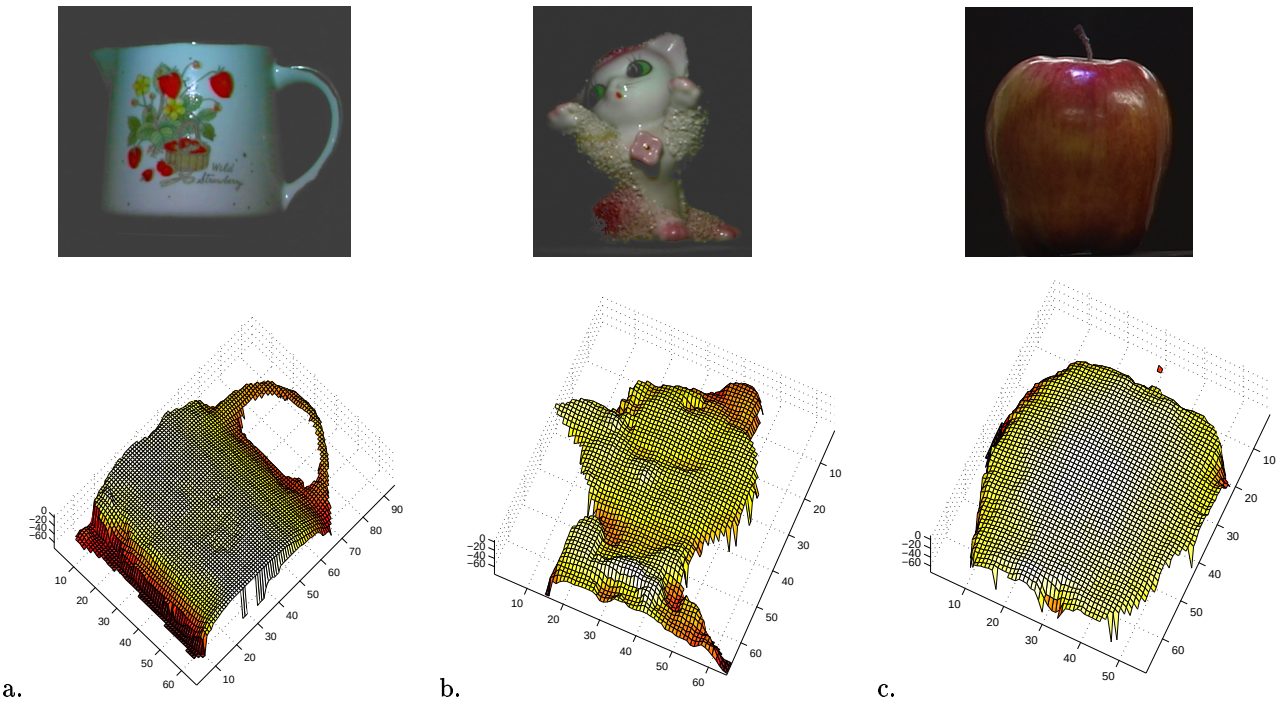

Figure 9: Some objects and their reconstructed depth maps - notice the highlights.

[4] D. Bhat and S. Nayar. Stereo and specular reflection. *Int. J. Computer Vision*, 26(2):91–106, 1998.

[5] I. J. Cox, S. Hingorani, B. M. Maggs, and S. B. Rao. Stereo without disparity gradient smoothing: a Bayesian sensor fusion solution. In *British Machine Vision Conference*, pages 337–346, 1992.

[6] D. Geiger, B. Ladendorf, and A. Yuille. Occlusions in binocular stereo. In *Proc. European Conf. on Computer Vision*, Santa Margherita Ligure, Italy, 1992.

[7] H. Hayakawa. Photometric stereo under a light-source with arbitrary motion. *J. Optical Society of America A*, 11(11):3079–3089, Nov. 1994.

[8] B. Horn. *Robot Vision*. MIT Press, Cambridge, Mass., 1986.

[9] K. Ikeuchi. Determining surface orientations of specular surfaces by using the photometric stereo method. *IEEE Trans. Pattern Anal. Mach. Intelligence*, 3(6):661–669, 1981.

[10] D. Jones and J. Malik. A computational framework for determining stereo correspondence from a set of linear spatial filters. In *Proc. European Conf. on Computer Vision*, Santa Margherita Ligure, Italy, 1992.

[11] J. Koenderink and A. van Doorn. Bidirectional reflection distribution function expressed in terms of surface scattering modes. In *Proc. European Conf. on Computer Vision*, pages II:28–39, 1996.

[12] J. Koenderink, A. vanDoorn, K. Dana, and S. Nayar. Bidirectional reflection distribution function of thoroughly pitted surfaces. *Int. J. Computer Vision*, 31(2/3):129–144, April 1999.

[13] M. Langer and S. W. Zucker. Shape-from-shading on a cloudy day. *J. Opt Soc. Am.*, pages 467–478, 1994.

[14] J. Lu and J. Little. Reflectance and shape from images using a collinear light source. *Int. J. Computer Vision*, 32(3):1–28, 1999.

[15] S. Magda, P. Belhumeur, and D. Kriegman. Shedding light on reconstruction and image-based rendering. In *SIGGRAPH Technical Sketch*, page 255, 2000.

[16] S. Nayar, K. Ikeuchi, and T. Kanade. Determining shape and reflectance of hybrid surfaces by photometric sampling. *IEEE J. of Robotics and Automation*, 6(4):418–431, 1990.

[17] M. Oren and S. Nayar. Generalization of the Lambertian model and implications for machine vision. *Int. J. Computer Vision*, 14:227–251, 1996.

[18] B. Phong. Illumination for computer-generated pictures. *Comm. of the ACM*, 18(6):311–317, 1975.

[19] W. Silver. *Determining Shape and Reflectance Using Multiple Images*. PhD thesis, MIT, 1980.

[20] H. Tagare and R. deFigueiredo. A theory of photometric stereo for a class of diffuse non-lambertian surfaces. *IEEE Trans. Pattern Anal. Mach. Intelligence*, 13(2):133–152, February 1991.

[21] K. Torrance and E. Sparrow. Theory for off-specular reflection from roughened surfaces. *JOSA*, 57:1105–1114, 1967.

[22] R. Woodham. Analyzing images of curved surfaces. *Artificial Intelligence*, 17:117–140, 1981.